arXiv:1602.07333v1 [nucl-th] 23 Feb 2016

February 25, 2016

Threshold pion production in proton-proton collisions at NNLO in chiral EFT

V. Baru,[1,2] E. Epelbaum,[1] A. A. Filin,[1] C. Hanhart,[3] H. Krebs,[1] and F. Myhrer[4]

[1] *Institut für Theoretische Physik II, Ruhr-Universität Bochum, D-44780 Bochum, Germany*

[2] *Institute for Theoretical and Experimental Physics, 117218, B. Cheremushkinskaya 25, Moscow, Russia*

[3] *Institut für Kernphysik, (Theorie) and Jülich Center for Hadron Physics, Forschungszentrum Jülich, D-52425 Jülich, Germany and Institute for Advanced Simulation, Forschungszentrum Jülich, D-52425 Jülich, Germany*

[4] *Department of Physics and Astronomy, University of South Carolina, Columbia, SC 29208, USA*

Abstract

The reaction $NN \to NN\pi$ offers a good testing ground for chiral effective field theory at intermediate energies. It challenges our understanding of the first inelastic channel in nucleon-nucleon scattering and of the charge-symmetry breaking pattern in hadronic reactions. In our previous studies, we presented a complete calculation of the pion-production operator for s-wave pions up-to-and-including next-to-next-to-leading order (NNLO) in the formulation of chiral effective field theory, which includes pions, nucleons and $\Delta(1232)$ degrees of freedom. In this paper we calculate the near threshold cross section for the $pp \to d\pi^+$ reaction by performing the convolution of the obtained operators with nuclear wave functions based on modern phenomenological and chiral potentials. The available chiral NN wave functions are constructed with a cutoff comparable with the momentum transfer scale inherent in pion production reactions. Hence, a significant portion of the dynamical intermediate-range physics is thereby cut off by them. On the other hand, the NNLO amplitudes evaluated with phenomenological wave functions appear to be largely independent of the NN model used and give corrections to the dominant leading order contributions as expected from dimensional analysis. The result gives support to the counting scheme used to classify the pion production operators, which is a precondition for a reliable investigation of the chirally suppressed neutral pion production. The explicit inclusion of the $\Delta(1232)$ is found to be important but smaller than expected due to cancellations.

I. INTRODUCTION

The investigation of near-threshold pion production in proton-proton collisions is important in order to gain insights into the dynamics involved in these first inelastic nucleon-nucleon (NN) scattering channels. The pion production reaction requires a relatively large three-momentum transfer and tests the applicability of chiral effective field theory (EFT) at intermediate energies. A good theoretical understanding of the isospin-invariant channels is an important prerequisite for investigations of charge symmetry breaking (CSB) in few-nucleon reactions such as e.g. the process $pn \to d\pi^0$, see recent review articles [1, 2] and references therein. The production of pions from two nucleons contributes as a building block to many few-nucleon processes [3, 4] and provides the dominant short-range mechanism in the three-nucleon force [5, 6]. It can be investigated experimentally and theoretically in inelastic nucleon-nucleon reactions, such as $pp \to d\pi^+$ and $pp \to pp\pi^0$. When the pioneering work of Koltun and Reitan [7] was confronted with the high-quality data of Meyer *et al.* [8], it was realized that the pion production dynamics was not well understood. Especially, the reaction $pp \to pp\pi^0$ appeared to be the most puzzling process. The experimentally measured cross section for this process [8] was found to be about ~ 5 times larger than the prediction of Ref. [7].

Low-energy pion dynamics is governed by the chiral symmetry of strong interactions and its breaking pattern. It thus can be naturally addressed in the framework of chiral EFT, see Refs. [9, 10] for pioneering studies along this line and Refs. [11–15] for more recent applications of chiral EFT to the pion-production reaction[1]. As mentioned, the measured near-threshold cross section for the neutral pion production channel is suppressed by almost an order of magnitude compared to charged pion-production channels. This suppression is naturally explained in chiral EFT [1, 2], where one finds the leading-order amplitude to $pp \to pp\pi^0$ to be numerically very small because the dominant isovector Weinberg-Tomozawa operator does not contribute. A quantitative understanding of neutral pion production therefore requires the inclusion of higher-order corrections [9, 10, 14, 15].

The reaction $pn \to d\pi^0$ is an important channel for the study of CSB in few-nucleon strong interactions [16]. Specifically, the experimentally measured differential-cross-section asymmetry [17] in this reaction has been computed using chiral EFT and was used to extract the strong-interaction contribution to the neutron-proton mass difference [18–20]. However, in order to extract reliably CSB observables, it is imperative to have an accurate description of the dominant isospin-symmetric amplitude and to ensure that the expansion of chiral EFT converges. To examine the convergence of chiral EFT, the $pp \to d\pi^+$ channel is a preferable reaction since: (i) unlike $pp \to pp\pi^0$, there is no suppressions of leading-order (LO) contribution in this charged pion production channel [7, 13–15], and (ii) precise experimental data from hadronic atom measurements are available [21, 22]. In this work we summarize the various contributions to the pion production operator, which were evaluated up to next-to-next-to-leading order (NNLO) in Refs. [14, 15], and calculate the $pp \to d\pi^+$ cross section near threshold in order to test the convergence of chiral expansion of chiral EFT.

Our paper is organized as follows. In section II we define the relations between observables and amplitudes in $pp \to d\pi^+$ channel. In section III we discuss the methods used to

[1] For an overview of the phenomenological approaches the interested reader is referred to the review articles Refs. [1, 2]

calculate the amplitudes for $NN \to NN\pi$ processes in the chiral EFT framework. In particular, we outline the counting scheme used to calculate pion production operators where the intermediate momentum transfer is larger than the pion mass. In section IV we discuss the complete NNLO operators for s-wave pion production given in the Appendix A. In Sections V and VI we perform a convolution of NNLO pion production operators with phenomenological and chiral NN wave functions, calculate observables, and compare them with experimental data. We summarize our findings in section VII.

II. THE $pp \to d\pi^+$ CROSS SECTION NEAR THRESHOLD

The differential cross section of the $pp \to d\pi^+$ reaction in the center-of-mass system (CMS) is expressed in terms of the transition amplitude as:

$$\frac{d\sigma}{d\Omega} = \frac{1}{64\pi^2}\frac{|\vec{q}_\pi|}{|\vec{p}_i|\,s}|\overline{M}|^2, \tag{1}$$

where $\vec{q}_\pi$ is the outgoing pion momentum, $\vec{p}_i$ is the incoming proton momentum, $\sqrt{s}$ is the total energy in CMS, and $|\overline{M}|^2$ is the square of the transition amplitude averaged over the spins of the initial protons and summed over the outgoing deuteron polarizations,

$$|\overline{M}|^2 = \frac{1}{4}\sum_{\lambda_1\lambda_2}\sum_{\epsilon_d}|M_{pp\to d\pi^+}(\lambda_1,\lambda_2,\vec{\epsilon}_d,\vec{p}_i,\vec{q}_\pi)|^2\,. \tag{2}$$

Here λ_1 and λ_2 are spin projections for each proton, and $\vec{\epsilon}_d$ is the deuteron polarization vector. At threshold, we can further simplify Eq. (1) using:

$$\sqrt{s} = m_d + m_\pi, \qquad |\vec{p}_i| = \sqrt{\frac{s}{4} - m_N^2}\,, \tag{3}$$

where m_N, m_d and m_π stand for the nucleon, deuteron and pion masses, respectively. To include the effects of NN interaction in the initial and final state it is convenient to perform a partial wave decomposition of the amplitude Eq. (2).

The total near threshold cross section of the $pp \to d\pi^+$ reaction in the center-of-mass system is conveniently parametrized as

$$\sigma = \alpha\eta + \beta\eta^3, \tag{4}$$

where η is the outgoing pion momentum in the units of the pion mass, i.e., $|\vec{q}_\pi| = \eta\, m_\pi$. The first term gives the outgoing s-wave pion contribution while the second one corresponds to an outgoing p-wave pion. At threshold, we only consider s-wave pion production, which means the cross section becomes $\sigma = \alpha\eta$, and the only contribution to α comes from the initial pp ${}^3P_1$ partial wave in spectroscopic notation. We denote the threshold transition amplitude[2] as M_{3P1}

$$M_{pp\to d\pi^+} \;=\; -\sqrt{\frac{3}{2}}M_{3P1}\,(\vec{\mathcal{S}}\times\hat{p}_i\,)\cdot\vec{\epsilon}_d{}^*\;,$$

[2] The amplitude M_{3P1} is related to the amplitude $\mathcal{B}$ used in Refs. [14, 15] as $M_{3P1} = 4i\mathcal{B}/\sqrt{3}$.

where the relevant spin-angular structure of the initial and final nucleon pairs are shown explicitly. Here $\vec{\mathcal{S}} = \chi_2^T \sigma_y \vec{\sigma} \chi_1/\sqrt{2}$ denotes the normalized spin structure of the initial spin-triplet state and $\hat{p}_i = \vec{p}_i/p_i$. We find

$$\alpha = \frac{4\pi}{64\pi^2} \frac{m_\pi}{p_i(m_\pi + m_d)^2} \frac{3}{4} |M_{3P1}|^2. \tag{5}$$

At threshold, the value of the parameter α can be extracted from the precise pionic deuterium lifetime experiment performed at PSI [21, 22], which has determined the total cross section for the channel $nn \to d\pi^-$ to be $\sigma(nn \to d\pi^-) = (252^{+5}_{-11})\eta\,\mu b$. Using this value and neglecting isospin breaking effects, we can extract the absolute value of the amplitude $|M_{3P1}|$ at threshold:

$$|M_{3P1}|^{\rm exp.} = 21.5^{+0.2}_{-0.5}. \tag{6}$$

The value of this amplitude will be compared with our chiral-EFT-based prediction to be presented below.

III. FORMALISM

The transition amplitudes for the $NN \to NN\pi$ processes involve several ingredients, namely the pion production operators from the two-nucleon system as well as NN bound and scattering states. Since the NN interaction is non-perturbative, these states cannot be directly calculated in chiral perturbation theory. Here and in what follows, we employ the hybrid approach suggested in [23]. The full amplitude is then calculated in two steps. First, the irreducible pion production operator is calculated perturbatively in the chiral EFT framework. In the second step, the resulting operator is convoluted with NN wave functions obtained from the solution of a non-perturbative Lippmann-Schwinger or Schrödinger equation with a realistic NN potential. We will also show results based on NN potentials derived in the framework of chiral EFT. It is important to ensure that the production operator itself does not contain any parts of NN interaction in order to avoid double counting. For this reason, only irreducible contributions to the production operator are considered, i.e. those which do not contain intermediate two-nucleon cuts. Notice that special care is required in order to isolate irreducible contributions if the production operator involves energy-dependent vertices, see Ref. [13] for more details.

The pion production operator is computed perturbatively in the framework of chiral EFT. It was shown in [10, 11, 24–29] that a naive application of the standard power counting rules, which treat all typical momenta p involved in a reaction on the same footing as the pion mass m_π, fails to reproduce the data and does not result in a convergent chiral expansion for the considered process. It was suggested in Refs. [9, 30] that the power counting should be modified to explicitly take into account the soft scale associated with typical transferred momenta $p \sim \sqrt{m_\pi m_N}$ in pion-production reactions. In the modified power counting which we refer to as the momentum counting scheme (MCS), the expansion parameter is

$$\chi_{\rm MCS} \simeq \frac{p}{\Lambda_\chi} \simeq \sqrt{\frac{m_\pi}{m_N}} \simeq \frac{m_\pi}{p}\,, \tag{7}$$

where $\Lambda_\chi \sim m_\rho \sim m_N$ (with m_ρ being the ρ meson mass) refers to the expected breakdown scale of the resulting chiral EFT approach.

Given the relatively high nucleon momenta in the initial state in the pion production reaction, it may be advantageous to include $\Delta(1232)$ as an explicit degree of freedom, see Refs. [30, 31] for the first steps in this direction and Refs. [32, 33] for earlier phenomenological calculations. Since the Δ-nucleon mass splitting $\delta = m_\Delta - m_N$ does not vanish in the chiral limit $m_\pi \to 0$, the resulting EFT has to be regarded as a phenomenological extension of chiral perturbation theory. A systematic treatment of the Δ resonance can be carried out using different counting rules, see e.g. Refs. [34, 35]. This is expected to result in more natural values of the low-energy constants (LECs) in the effective Lagrangian and an improved convergence of the EFT expansion. Here and in what follows, we utilize the approach of Ref. [12] and count the Δ-nucleon mass splitting within the MCS as $\delta \sim p \sim \sqrt{m_\pi m_N}$. Further, to systematically investigate the role of the Δ isobar in the considered process, we will implement different calculational strategies which are briefly outlined below.

- The most complete treatment of the Δ isobar is achieved by using the Δ-full formulation of chiral EFT, which is based on the effective Lagrangian for pions, nucleons and Δ isobars, and by including Δ-excitations in the Hilbert space which results in a coupled-channel framework. The initial state interaction then includes the $NN \to N\Delta$ transition and, consequently, the pion-production operator involves a contribution from the $N\Delta \to NN\pi$ channel[3]. A coupled-channel extension of the NN amplitudes to account for the $NN \to N\Delta$ transitions was developed in Ref. [36] on the basis of the CD Bonn potential. Another model, the CCF model, uses the coupled-channel folded diagrams formalism to include $NN \to NN$ and $NN \to N\Delta$ transitions, see Ref. [37]. The resulting framework will be referred to as the coupled-channel Δ-full chiral EFT approach (CCχEFT$-\Delta$).

- The coupled-channel formulation described above does explicitly take into account the momentum scale $\sim \sqrt{(m_\Delta - m_N)m_N}$ corresponding to real Δ excitations in NN collisions. This (numerically) rather high momentum scale can be integrated out. The coupled-channel treatment can then be avoided by perturbatively including all effects associated with the Δ-nucleon mass difference δ in the pion production operator and requiring that the Hilbert space consists of only nucleonic states. The resulting formulation will be referred to as the Δ-full chiral EFT approach (χEFT$-\Delta$). Notice that the contributions to the scattering amplitude which distinguish between the CCχEFT$-\Delta$ and χEFT$-\Delta$ approaches were argued in Ref. [15] to be of a higher order than the one considered in our calculation. Since most of the modern phenomenological and chiral NN potentials do not include the $NN \to N\Delta$ transition explicitly, we will use this strategy to study the influence of different NN wave functions on the results. (We also will give results based on the coupled-channel extension of the CD Bonn potential of Ref. [36].)

- Meanwhile, one may integrate out the Δ degrees of freedom already at the level of the effective Lagrangian which leads to the standard Δ-less formulation of chiral EFT to be referred as χEFT$-\not\Delta$. In this formulation, all effects of the Δ-resonance are implicitly taken into account via the LECs of the effective Lagrangian.

[3] The intermediate $\Delta\Delta$ state is suppressed in our power counting [15] and therefore not included explicitly in the coupled-channel formalism.

It is important to keep in mind that (i) the LECs have a different meaning and take different values in the Δ-full and Δ-less formulations of chiral EFT and (ii) the contributions to the irreducible pion production operator are different in all three approaches. More precisely, the production operator involves only diagrams with nucleon lines in the χEFT$-\not{\Delta}$ approach, while diagrams involving Δ isobars may yield different contributions in the CCχEFT$-\Delta$ and χEFT$-\Delta$ formulations due to the different meaning of irreducibility. This issue will be discussed in detail in the next section.

Finally, the convolution of the production operator with the initial and final NN wave functions is done by first performing a partial wave projection of the pion-production operator. The resultant operator is sandwiched between the NN wave functions and integrated up to a momentum cutoff of order 600–1000 MeV which is of the order of the expected breakdown scale of the chiral EFT. The equations defining the convolution procedure are given in Appendix A of Ref. [15].

IV. THE S-WAVE PION-PRODUCTION OPERATOR IN χEFT$-\Delta$

We have calculated the expressions for the pion production operator relevant for s-wave pion production up-to-and-including NNLO in MCS within the χEFT$-\Delta$ formulation. The complete expressions for the operators were derived in Ref. [15] and are given in the Appendix A of this work, while in this section we summarize the most important results. Notice further that the expressions for the production operator in the χEFT$-\not{\Delta}$ formulation can be obtained by simply dropping the Δ contributions provided we redefine some of the LECs.

Only two types of diagrams contribute to the dominant LO operators, the single-nucleon "direct" pion production operator and the Weinberg-Tomozawa operator (including its recoil correction labelled WT recoil), illustrated in the top row in Fig. 1. At next-to-leading order (NLO), the tree-level diagrams with intermediate Δ excitations start to contribute (first two diagrams in the second row in Fig. 1 labelled as "dirΔa" and "dirΔb"). In addition, loop diagrams appear at NLO. However, as was shown in Refs. [12, 13], the sum of all NLO loop diagrams illustrated in the third row in Fig. 1 cancel exactly for s-wave pion production. Refs. [12, 15] showed that also the NLO loop diagrams with an intermediate Δ shown in the fourth row in Fig. 1 cancel exactly. Meanwhile, there are also non-vanishing contributions of the loop diagrams shown in the second row in Fig. 1 (diagrams "ΔBox a" and "ΔBox b"). The contributions of these box diagrams do not vanish if the $\pi N \to \pi N$ vertex is taken on shell, that is it should be proportional to $2m_\pi$ in full analogy to the Weinberg-Tomozawa operator at LO. Naively, these operators appear to be suppressed according to the MCS and formally start to contribute at NNLO. On the other hand, these two "box" diagrams are exceptional among loop operators in the sense that their contributions are potentially enhanced due to the presence of a (reducible) $N\Delta$ intermediate state. Indeed, due to the relatively small mass difference between the nucleon and Δ, the $N\Delta$ propagator at the pion production threshold effectively scales as

$$\frac{1}{m_\pi - \delta - p^2/m_N} \sim \frac{1}{m_\pi}, \tag{8}$$

in contrast to a $1/\delta \sim 1/p$ behavior expected from an MCS estimate. This might lead to an enhancement compared to the expected MCS contribution of these box diagrams. This argument is supported by the explicit calculations presented in Sec.V B. Following this logic, we promote these two particular box diagrams to NLO, i.e. to the order where there are

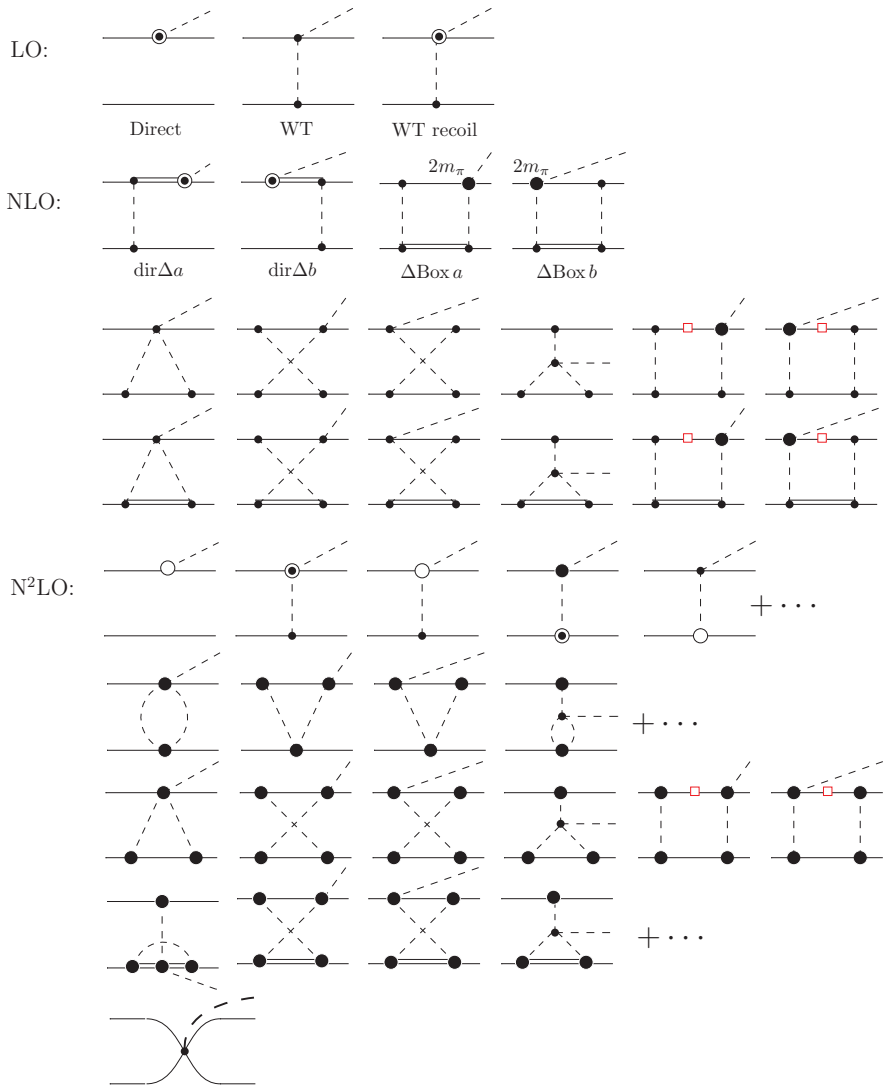

FIG. 1: Diagrams contributing to the s-wave pion-production operator up to NNLO in χEFT$-\Delta$. Dashed, solid and double lines denote pions, nucleons and Δ-resonance, respectively. The complete expressions for the vertices and the corresponding Lagrangians are given in Ref. [15]. Solid dots refer to vertices from the leading-order Lagrangians $\mathcal{L}^{(1)}_{\pi N}$ and $\mathcal{L}^{(2)}_{\pi\pi}$ while vertices denoted by the symbol $\odot$ originate from the sub-leading Lagrangian $\mathcal{L}^{(2)}_{\pi N}$. Filled circles indicate the possibility to have both leading and sub-leading vertices from $\mathcal{L}^{(1)}_{\pi N}$ and $\mathcal{L}^{(2)}_{\pi N}$ in the diagram, see Fig. 2 in Ref. [15] for clarification. Open circles refer to vertices from $\mathcal{L}^{(3)}_{\pi N}$ while red squares on the nucleon propagator in the box diagrams indicate that the corresponding nucleon propagator cancels with parts of the πN vertex and leads to the irreducible contribution, see Ref. [15] for further details. The last NNLO diagram is the five-point contact term (CT) diagram.

other (tree-level) diagrams with the $N\Delta$ intermediate state shown in the second line in

Fig. 1[4]. This treatment of these diagrams is consistent with that used in [38–40] to calculate the corrections to the pion deuteron scattering length due to the $\Delta(1232)$. In particular, it was shown in Ref. [38] that both contributions from the "direct" pion emission via the intermediate $\Delta(1232)$ excitation (the diagrams similar to the first two in the second line in Fig. 1) and the Δ-box diagrams involving the Weinberg-Tomozawa on shell $\pi N \to \pi N$ vertex are roughly of similar size.

Finally, at NNLO there are tree-level and loop diagrams as well as the five-point contact terms (CTs) contributing to the pion production operator. Specifically, there is one contact term in the reaction channel $pp \to d\pi^+$ and another in $pp \to pp\pi^0$. In addition, there are numerous NNLO loop diagrams with explicit Δ's. Only some of these loop diagrams are illustrated in Fig. 1. We have calculated all diagrams and found numerous cancellations among the loop contributions at NNLO [15]. Unlike NLO loop diagrams (see rows 3 and 4 in Fig. 1), where the cancellation is exact, a finite contribution remains after renormalization of the operators at NNLO. We also find a finite contribution from the NNLO tree-level diagrams. The complete set of analytic expressions for the NNLO pion production operators is given in Ref. [15] and is summarized in appendix A.

In the next section we consider the contributions of these operators to the $pp \to d\pi^+$ threshold amplitude and compare them with the experimentally determined amplitude in Eq. (6). As should be clear from the discussion in this section, our calculation is parameter free up-to-and-including NLO, while at NNLO there is one contact term which can always be adjusted to compensate the deviation from the experimental amplitude at threshold. The goal of the study, however, is to demonstrate that the counting scheme used to classify the operators is adequate, i.e. the size of the operators which appear at the given order is in agreement with the estimate. This is a precondition for a reliable estimate of the theoretical uncertainty and is also needed to correctly identify the production mechanism in the chirally suppressed $pp \to pp\pi^0$ channel. In order to comply with this goal, in the next section we discuss the contribution of the NNLO operators without the NNLO contact term and compare this result with the estimate expected based on Eq. (7). Further, from the difference between the NNLO theoretical prediction (without the contact term) and the data, we extract the value of the contact term contribution and again confront it with the estimate.

V. NUMERICAL RESULTS

We calculate the threshold amplitude $M_{^3P1}$ for the reaction $pp \to d\pi^+$ by performing the convolution of pion production operators of section IV (see Fig. 1 and also the appendix A) with a set of NN wave functions derived from the modern phenomenological potentials: CD Bonn [41], Nijmegen [42] and AV18 [43]. In what follows, the expression for the $NN \to NN\pi$ operator, which is derived based on the diagrams shown in Fig. 1, will be called the (s-wave) *pion production operator* while its convolution with the NN interaction in the initial and final state will be referred to as the (s-wave) *pion production amplitude*. In this section we discuss the results of the convolution and compare the resulting amplitudes with the value extracted from experiment in Eq. (6). In our momentum space evaluations of the production

[4] Note that only the diagrams in the second row in Fig. 1, involving an "initial" Δ, i.e. dirΔa and ΔBox a, contribute to $pp \to d\pi^+$ while all four diagrams are relevant for $pp \to pp\pi^0$.

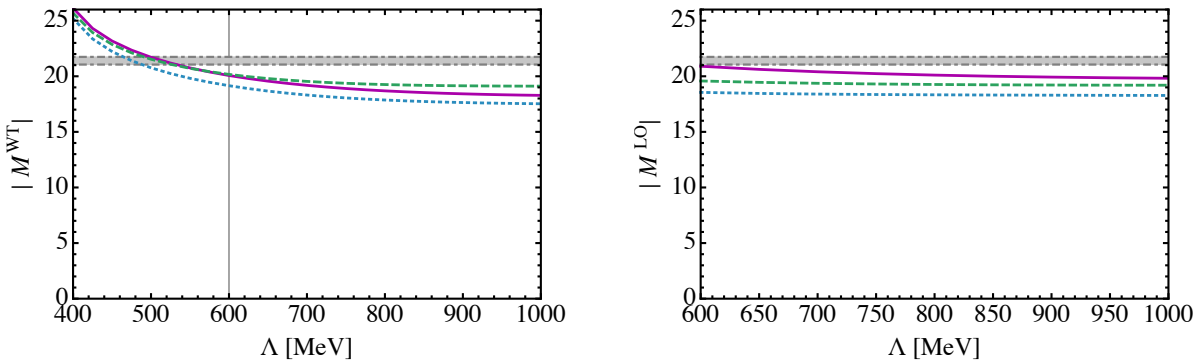

FIG. 2: The $pp \to d\pi^+$ amplitude $|M_{^3P_1}|$ calculated based on solely the LO Weinberg-Tomozawa operators (left panel) and all LO operators (right panel) as a function of a sharp momentum integral cutoff Λ. The amplitude is calculated using various *phenomenological* NN wave functions: solid violet line — CD Bonn [41], dashed green — Nijm 1 [42], dotted blue — AV18 [43]. The vertical line in the left panel indicates the value of the cutoff (about 600 MeV) where amplitude becomes (almost) cutoff independent. The horizontal grey band between the dot-dashed lines shows the experimental value of the amplitude $|M_{^3P_1}|$ including the errors (see Eq. (6)) extracted from Refs. [21, 22].

amplitude, the convolution integrals are supplied with a sharp ultraviolet cutoff Λ, which will be varied in a certain range.

To test the convergence of chiral EFT, we find it instructive to consider the contributions of the various pion-production operators, given in the appendix A, separately. We start the discussion with the long-range leading-order pion-production operator corresponding to the diagrams WT and WT recoil in Fig. 1 involving the Weinberg-Tomozawa vertex. This LO operator is known [13] to give the most important contribution to the amplitude $M_{^3P_1}$. In the left panel of Fig. 2, we show the contribution to the amplitude from the WT diagrams as a function of the cutoff Λ calculated using various phenomenological NN wave functions. As expected for a long-range operator, the observable has almost no dependence on the NN interaction model for $\Lambda \geq 600$ MeV. The cutoff-dependence for small cutoff values in the range 400–600 MeV is not surprising since the typical momentum transfer in the pion production is about 360 MeV. Therefore, for cutoffs less than about 600 MeV, the separation of intermediate and short distance scales becomes insufficient to get fully cutoff-independent results. In what follows we consider cutoff values in the range $\Lambda = 600$–1000 MeV.

Next, we consider the complete leading-order result. In addition to the WT operator (and its recoil correction), there is one more diagram at LO, which is known as the direct pion production operator (Fig. 1). Since this is a single-nucleon operator, which probes the NN interaction at shorter distances, it is natural to expect that the total LO amplitude might become more sensitive to the short-range details of the different NN models. However, the contribution of the direct term is known to be very small due to a destructive interference between the Born term and the contribution of the NN initial state interaction, see e.g. Ref. [13] where this interference was shown for CCF [37] and CD Bonn [41] potentials. As a consequence, the direct pion production operator does not introduce any apparent cutoff dependence for the three NN potentials as can be seen in the right panel of the Fig. 2. The evaluated complete LO amplitude is close to but smaller than the experimental value for $M_{^3P_1}$ in Eq. (6) for all phenomenological NN potentials used in our calculations.

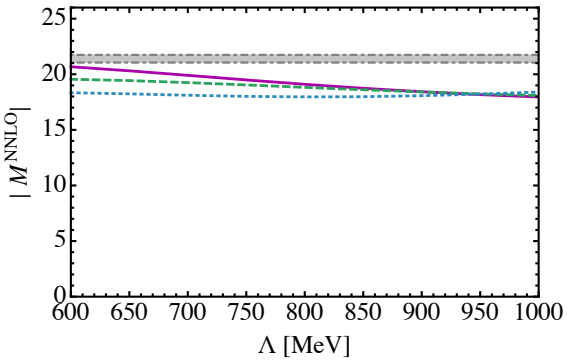

FIG. 3: The $pp \to d\pi^+$ amplitude $|M_{3P1}|$ as a function of the cutoff calculated using the complete set of LO, NLO and NNLO operators except for the NNLO five-point contact term operator. The amplitude is calculated using several *phenomenological* NN wave functions, see Fig. 2 for notation. The difference between experimental and evaluated amplitudes determines the required strength of the unknown five-point NNLO contact term in order for the theory to fit the data.

We are now in the position to consider the complete pion production amplitude including all LO, NLO and NNLO pion production operators introduced in section IV. First, we note that all NLO operators from the loop diagrams were shown to cancel exactly in Ref. [13]. This cancellation also applies to the NLO loop diagrams involving the intermediate Δ as shown in Ref. [15] (fourth row of diagrams in Fig. 1). Further, the tree-level NLO operators from diagrams in the second row of Fig. 1 show a destructive interference with the corresponding Δ-box terms and their net contribution is small, see Sec.V B for a more detailed discussion of this cancellation.

Apart from the unknown LEC of the five-point CT (last diagram in Fig. 1), we need to specify the values of the LECs c_i, $i = 1, \ldots, 4$, in our evaluation of the production amplitude at NNLO. The values for the c_i's are taken from a tree-level order fit (chiral order Q^2 fit 1) to πN scattering data, Ref. [44]. The sensitivity to the choice of these LECs is discussed in Sec. V A.

In Fig. 3 we show the pion production amplitude up-to-and-including NNLO as a function of the cutoff. Comparing the results in Figs. 2 (right) and 3, we conclude that the NNLO amplitude contributes up to 10% to the amplitude $|M_{3P1}|$. This result shows that the perturbative treatment of the production operator is reasonable and supports the counting scheme used to classify the pion production operators. We also observe from Fig. 3 that the results for all phenomenological NN models are in a reasonably good agreement with each other — the changes in the results due to the use of different NN models and from the cutoff variations are well within the NNLO estimates based on the MCS. We emphasize, however, that the contribution of the NNLO contact term (CT) [see last row in Fig. 1] is not included. As usual in EFT, this contact term is expected to compensate for this (already rather mild) cutoff dependence as well as for the natural dependence of the results from different NN-models. The difference between the calculated pion production amplitude, which contains all LO, NLO and NNLO operators, and the experimental value of $|M_{3P1}|$ (shown as a horizontal dashed-dotted band) illustrates the magnitude of the CT amplitude required to reproduce the data. In chiral EFT, the CT operators parameterize the contributions from short-range processes, which are not treated as explicit degrees of freedom. For example, short-range contributions due to exchange of the vector-mesons ρ- and ω are implicitly accounted for via

the corresponding NNLO CT operator in our chiral EFT. A fit to the data reveals that the contribution of the counter term is of the order of 5–15% of the LO contribution (depending on the NN model used) which is consistent with the power counting. Finally, from the comparison of the LO result in Fig. 2 (right) with the experimental data, we conclude that the net contribution from all NNLO operators (including the contact term) is very small and fully in line with the power counting.

A. Sensitivity to the LECs c_i

We now address the sensitivity of the pion production amplitude to the values of the LECs c_i. As already mentioned, the results shown in Fig. 3 are obtained with the c_i values determined from a tree-level order fit (chiral order Q^2 fit 1) to πN scattering data [44] in a theory with an explicit Δ, namely

$$c_1 = -0.57 \text{ GeV}^{-1}, \quad c_2 = -0.25 \text{ GeV}^{-1}, \quad c_3 = -0.79 \text{ GeV}^{-1}, \quad c_4 = 1.33 \text{ GeV}^{-1}. \quad (9)$$

These values correspond to the $\pi N\Delta$ decay constant $g_{\pi N\Delta} = 1.34$.

On the other hand, the values of the c_i's emerging from one-loop calculations of πN scattering are well-known to be significantly different [45–51]. For a discussion of the LECs c_i extracted from NN analyses we refer to Ref. [52]. Notice further that pion-nucleon scattering phase shifts were recently determined in the framework of the Roy-Steiner equation which takes into account constraints from analyticity, unitarity, and crossing symmetry [53]. It is conceivable that this analysis will allow for a more accurate determination of the c_i's in the future, see [54] for a first step along this line. To have an idea of the sensitivity of our results to the values of these LECs, we consider the empirical values of

$$c_1 = -0.81 \text{ GeV}^{-1}, \quad c_2 = 3.28 \text{ GeV}^{-1}, \quad c_3 = -4.69 \text{ GeV}^{-1}, \quad c_4 = 3.40 \text{ GeV}^{-1}, \quad (10)$$

which have been used in the new generation of chiral NN potentials at NNLO and N^{3}LO of Ref. [52]. Except for c_2, these values correspond to the analysis of πN scattering inside the Mandelstam triangle of Ref. [55], where the chiral expansion is expected to converge faster than in the physical region. The value of c_2, which could not be determined reliably in Ref. [55], is taken from the one-loop Q^3 calculation of Ref. [45]. Given that the values of the c_i's in Eq.(10) have been obtained in the standard formulation of chiral perturbation theory based on pions and nucleons as the only explicit degrees of freedom, we have to subtract the leading Δ contributions in order to be able to use the LECs in χEFT$-\Delta$. Using the well-known Δ contributions discussed in Ref. [56], we arrive at the values of

$$c_1 = -0.81 \text{ GeV}^{-1}, \quad c_2 = 0.56 \text{ GeV}^{-1}, \quad c_3 = -1.97 \text{ GeV}^{-1}, \quad c_4 = 2.04 \text{ GeV}^{-1}. \quad (11)$$

These numbers are used in our calculation together with $g_{\pi N\Delta} = 1.34$.

In Fig.4 we illustrate the effect of the variations of the LECs c_i on the $pp \to d\pi^+$ amplitude. For this purpose, we calculate the pion-production amplitude as a function of the cutoff with the two sets of the c_i's as specified in Eqs. (9) and (11) for several NN potentials. Specifically, the red band is restricted by two solid lines obtained using the three different NN models corresponding to the AV18, Nijm1 and CD Bonn potentials [41–43], with the order Q^2 values of the c_i's from Eq. (9). Similarly, the blue band is calculated with the same NN potentials but with the empirical values of the c_i's from Eq. (11). We conclude that the difference between the bands lies well within the uncertainty estimate expected at order NNLO.

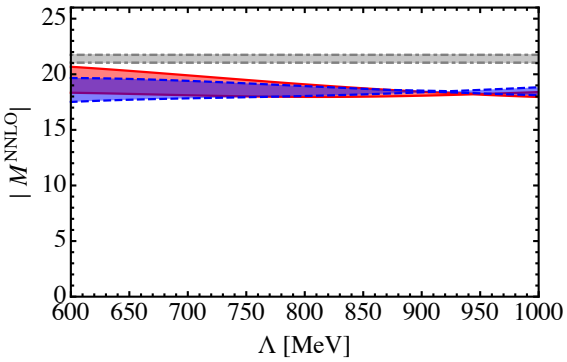

FIG. 4: Sensitivity of the $pp \to d\pi^+$ amplitude to the choice of the LECs c_i. The red band restricted by two solid lines corresponds to the results obtained with the order-Q^2 values of the c_i's specified in Eq. (9) for three phenomenological NN potentials (AV18, Nijm1 and CD Bonn). The blue band between the dashed lines is obtained using the empirical values of the c_i's [52, 55] with the Δ contributions being subtracted as specified in Eq. (11) and employing the same NN wave functions. The NNLO contact term is not included. See Sec. V A for a more complete discussion and Fig. 2 for notation of the horizontal grey band.

B. Effects of the $\Delta(1232)$ on the threshold pion-production amplitude

As discussed in Sec. III, the inclusion of the Δ degree of freedom in the theory may be accomplished using the two different strategies described in Sec. III. The results already presented correspond to the χEFT$-\Delta$ formulation, where the contributions of the Δ resonance are perturbatively incorporated into the pion-production operator as shown in the second row in Fig. 1. This operator is then sandwiched by the initial and final NN state wave functions. Note that the $NN - N\Delta$ transition, which naturally appears as a part of the pion-production operator, contains a contact term in addition to the one-pion exchange (OPE) potential. However, this contact term appears to be suppressed by $\chi^2_{\rm MCS}$ (see Eq. (7)) relative to the OPE potential, since it comes with at least two derivatives as a consequence of the Pauli principle (see, e.g., Ref. [57] for a related discussion). Since the Δ in $NN \to NN\pi$ starts to contribute at NLO, to the order we are working, the unknown short range part in the $NN \to N\Delta$ transition can be dropped. Hence, only the diagrams shown in the second row in Fig. 1 are relevant.

In the CCχEFT$-\Delta$ formulation, the initial NN and $N\Delta$ states are generated non-perturbatively. The corresponding elastic $NN \to NN$ and inelastic $NN \to N\Delta$ transition amplitudes are obtained as a solution of the coupled-channel system with NN and $N\Delta$ interactions

$$\begin{aligned} T_{\rm NN} &= V_{\rm NN} + V_{\rm NN} G_{\rm NN} T_{\rm NN} + V_{\rm NN-N\Delta} G_{\rm N\Delta} T_{\rm N\Delta-NN}, \\ T_{\rm N\Delta-NN} &= V_{\rm N\Delta-NN} + V_{\rm N\Delta-NN} G_{\rm NN} T_{\rm NN} + V_{\rm N\Delta-N\Delta} G_{\rm N\Delta} T_{\rm N\Delta-NN}, \end{aligned} \tag{12}$$

where $G_{\rm NN}(G_{\rm N\Delta})$ is the NN ($N\Delta$) Green-function and $V_{\rm NN}$, $V_{\rm N\Delta-N\Delta}$, and $V_{\rm N\Delta-NN}$ are the corresponding elastic and transition potentials, respectively. The short-range parts of the $N\Delta$ and $\Delta\Delta$ interactions are constrained by fitting the NN observables [36, 37]. Since the NN and $N\Delta$ states are coupled, the full pion-production amplitude also receives contributions from diagrams containing initial and final $N\Delta$ states as shown in Fig. 5. In a full analogy to the "direct" single-nucleon diagrams in Fig. 1, diagrams shown in Fig. 5 do

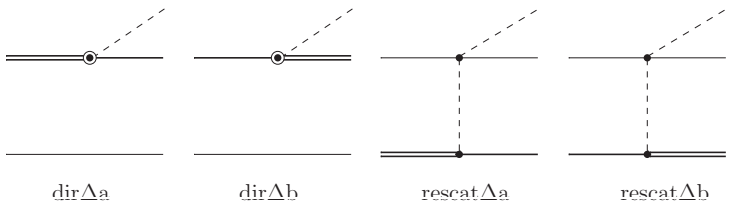

FIG. 5: Additional diagrams contributing to the production operator in the CCχEFT$-\Delta$ formulation. In the last two rescattering diagrams, only the on-shell part of the πN scattering vertex ($2m_\pi$) should be included [15]. Note that only the diagrams, which contain Δ in the initial state, i.e., dirΔa and rescatΔa, contribute to the reaction $pp \to d\pi^+$.

not contribute to the on-shell pion-production operator but have to be taken into account when convolved with the $NN - N\Delta$ wave functions either in the initial or in the final state. Notice that for the $pp \to d\pi^+$ reaction, the $NN - N\Delta$ transition can only appear in the initial state due to isospin conservation. To avoid double counting, all diagrams shown in the second row in Fig. 1 have to be dropped when calculating the production operator in the CCχEFT$-\Delta$ formulation.

We now compare the results of both Δ-full formulations with each other and with the results using the Δ-less approach. For the sake of a meaningful comparison, we use here the wave functions based on the CD Bonn potential [41] and on the coupled-channel version of the CD Bonn potential [36]. The resulting values of the pion production amplitude $M_{^3P1}$, which do not include the contribution of the $NN \to NN\pi$ counter term, are collected in Table I. The calculations are done with the cutoff $\Lambda = 1$ GeV. Notice that the results with the explicit Δ degree of freedom (χEFT$-\Delta$ and CCχEFT$-\Delta$ in Table I) are obtained using the order-Q^2 values for the c_i's in Eq. (9), whereas in the Δ-less approach (χEFT$-\not{\Delta}$) we take the corresponding order-Q^2 values which include the contributions of the Δ isobar, namely [44]:

$$c_1 = -0.57 \text{ GeV}^{-1}, \quad c_2 = 2.84 \text{ GeV}^{-1}, \quad c_3 = -3.87 \text{ GeV}^{-1}, \quad c_4 = 2.89 \text{ GeV}^{-1}. \qquad (13)$$

We find that the coupled-channel approach (CCχEFT$-\Delta$) yields the amplitude which is about 12% larger than the one in the χEFT$-\Delta$ formulation. This difference is comparable with an estimate of the NNLO contributions based on the MCS. This result indicates that the coupled-channel dynamics and the inclusion of the short-range $N\Delta$ interaction, constrained by the NN data, is somewhat more important than what is expected based on dimensional analysis. As shown in Table II, this difference can be attributed to the contributions from the diagrams shown in the second row in Fig. 1 and in Fig. 5, all involving the intermediate $N\Delta$ state.

The contributions from the diagrams dirΔa and ΔBox a in Fig. 1 are relatively large in the χEFT$-\Delta$ framework, as expected at NLO in the MCS, but they interfere destructively. The contributions of the direct and rescattering diagrams (dirΔa and rescatΔa) in the CCχEFT$-\Delta$ approach are smaller individually than in the previous case, but they also undergo significant cancellations in the sum. This finding was also observed in Ref. [31] using the CCF model [37]. The pattern shown in Table II could have been expected: as is known from phenomenological studies, the destructive interference between tensor parts of the OPE and short range potentials leads to smaller amplitudes in the coupled-channel framework as compared to a perturbative treatment where no short-range term is included. As shown

TABLE I: The results for the amplitude M_{3P1} calculated for three different strategies with respect to the treatment of the Δ, as discussed in the text. The results correspond to the cutoff $\Lambda = 1$ GeV.

CCχEFT$-\Delta$	χEFT$-\Delta$	χEFT$-\not{\Delta}$
$18.1 - 9.6i$	$16.0 - 8.5i$	$16.5 - 8.8i$

TABLE II: Individual contributions to the amplitude M_{3P1} from the diagrams with reducible $N\Delta$ intermediate states, as shown in Figs. 5 (dirΔa and rescatΔa) and 1 (dirΔa and ΔBox a), after the convolution with the appropriate initial state wave functions. Diagrams "b" in the corresponding figures do not contribute to the reaction channel with the isospin 0 (deuteron) final state. Except those diagrams discussed above, the net contribution of all other diagrams in Fig. 1 is labelled as "All other diagrams". The results correspond to the cutoff $\Lambda = 1$ GeV.

CCχEFT$-\Delta$	χEFT$-\Delta$
dir$\Delta a = 2.8 - 1.5i$	dir$\Delta a = 4.8 - 2.5i$
rescat$\Delta a = -1.9 + 1.0i$	ΔBox $a = -6.1 + 3.2i$
All other diagrams$= 17.3 - 9.2i$	All other diagrams$= 17.3 - 9.2i$

in Table II, the net contribution of the operators with the $N\Delta$ intermediate state appears to be small in both cases but has an opposite sign. This sign difference accounts for the deviation between the results of two Δ-full approaches. Interestingly, the net contribution from all other operators in Fig. 1, apart those with the $N\Delta$ intermediate state discussed above, appears to be almost insensitive to whether NN interaction in the initial state is treated using a full coupled-channel approach (CCχEFT$-\Delta$) or the Hilbert state consists of only nucleonic states while Δ is included perturbatively (χEFT$-\Delta$). Finally, as seen in Table I, if the Δ degree of freedom is integrated out at the level of the effective Lagrangian (χEFT$-\not{\Delta}$), the result for the reaction amplitude at $\Lambda \simeq 1$ GeV is about 10% smaller compared to the CCχEFT$-\Delta$ formalism but only a few percent larger than the one in the χEFT$-\Delta$ framework. It should be noted at this point that for the cutoff $\Lambda \simeq 1$ GeV the amplitudes discussed in Table I are already largely saturated. On the other hand, at smaller cutoffs the NNLO amplitudes, which do not yet include the $NN \to NN\pi$ contact term contribution, are expected to possess some cutoff dependence. The individual numbers shown in Tables I and II may therefore change. However, the destructive interference pattern discussed above generally persists. Due to this interference, the difference between the Δ-full and Δ-less approaches, which is estimated to be of the size of NLO terms, is smaller for cutoffs $\Lambda \geq 700$ MeV. Moreover, the deviation in the results for all three approaches constitutes generally an NNLO effect in this range of cutoffs.

It should be noted, however, that the cancellation discussed above is probably a particular feature of s-wave pion production in $pp \to d\pi^+$ channel. For example, the p-wave pion production amplitudes in this reaction channel (especially the dominant amplitude in the ${}^1D_2 \to {}^3S_1 p$ partial wave) do acquire a large (NLO) contribution from diagram dirΔa in Fig. 1 [4] while box diagram ΔBox a starts to contribute at next-to-next-to-next-to-leading order (NNNLO) only and therefore is expected to be suppressed. It remains to be seen if the cancellation discussed above takes place for s-wave pion production in $pp \to pp\pi^0$ channel.

VI. CONVOLUTION WITH CHIRAL NN POTENTIALS

In this section we consider the convolution of pion-production operators with NN wave functions generated by potentials derived in chiral EFT. Certainly, this approach is more consistent from the conceptual point of view than the hybrid method employed in the previous sections since all ingredients are calculated based on the same effective Lagrangian. On the other hand, the available chiral nuclear potentials are actually derived in the formulation of chiral EFT, where the momentum scale $p \sim \sqrt{m_N m_\pi}$ associated with radiative pions and relevant for the pion production reaction is integrated out. Thus, it is, in fact, more appropriate to also regard such calculations as of being a hybrid type in spite of the fact that the corresponding NN wave functions are calculated in the framework of chiral EFT. Furthermore, the soft nature of chiral EFT potentials corresponding to lower values of the momentum-space cutoff Λ_{NN} as compared with phenomenological potentials suggests a possible appearance of significant finite-Λ_{NN} artefacts. We further emphasize that the initial energy corresponding to the pion production threshold is at the very edge of the applicability range of even the state-of-the-art fifth-order chiral potentials of Ref. [58].

Here and in what follows, we will use the new generation of NN potentials up to fifth order ($\mathrm{N^4LO}$) in the chiral expansion presented in Refs. [52, 58]. In contrast to the first-generation chiral $\mathrm{N^3LO}$ NN forces of Refs. [59, 60], the new potentials utilize a coordinate-space regularization scheme for long-range components which reduces the amount of finite-regulator artefacts. The employed coordinate-space cutoff is varied in the range $R = 0.8 \ldots 1.2$ fm, which in momentum space roughly corresponds to cutoffs of the order of $\Lambda_{NN} \sim 500 \ldots 330$ MeV. In contradistinction to the exponentially falling high-momentum behavior of the older chiral potentials, the new chiral potentials used in this work have a power-like momentum cut-off. The new chiral potentials preserve the correct analytic structure of the amplitude at low energies and lead to a good description of deuteron properties and NN phase shifts for the harder cutoff choices of $R = 0.8 \ldots 1.0$ fm. For the two softest choices of the regulator with $R = 1.1$ fm and $R = 1.2$ fm, one observes significant regulator artefacts (especially at higher energies), see Refs. [52, 58] for more details. Notice further that the corresponding values of the momentum-space cutoff, $\Lambda_{NN} \sim 360$ MeV and $\Lambda_{NN} \sim 330$ MeV, are comparable with or even smaller than the momentum transfer scale $p \sim \sqrt{m_N m_\pi} \sim 360$ MeV inherent in pion production reactions. This proximity of scales indicates that the corresponding potentials are actually too soft for the purpose of applications to the pion production reaction. Even for the hardest available choice of the regulator in the new chiral NN potentials, one may expect that a significant portion of the dynamical intermediate-range physics is effectively transferred from the NNLO amplitude to the NNLO contact term, which is thus enhanced compared to the evaluation in the previous sections. In order to explicitly show the effects of such low-momentum cutoffs, we calculate the pion-production amplitude using the convolution of the operators from Sec. IV with chiral NN wave functions.

We again first consider the long-range LO WT contribution to the pion-production operator. The result of its convolution with chiral wave functions is shown in Fig. 6 (left). As expected, the amplitudes are very similar to the ones obtained with phenomenological potentials (cf. Fig. 2 left). We next consider the complete LO operator including the direct term. The inclusion of the LO direct pion production operator yields the amplitude shown in the right panel of Fig. 6. We see that the contribution of the direct operator is no longer small (compared to the calculation with phenomenological NN wave functions Fig. 3). Furthermore, as expected, the inclusion of the direct term generates a dependence

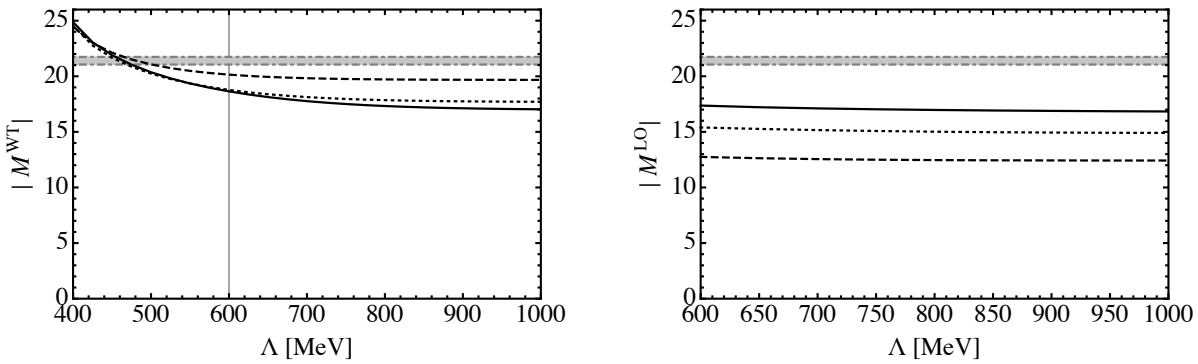

FIG. 6: The $pp \to d\pi^+$ amplitude $|M_{^3P1}|$ based solely on the LO Weinberg-Tomozawa operator (left panel) and all LO operators (right panel) as a function of the sharp momentum integral cutoff Λ. The amplitude is calculated using the *chiral* NN wave functions at N^{4}LO for different choices of the regulator, namely $R = 0.8$ fm (solid orange line), $R = 1.0$ fm (dotted orange line) and $R = 1.2$ fm (dashed orange line). See Fig. 2 for notation of the horizontal grey band.

on the short-range details of the chiral NN potentials. One can clearly see the pattern: chiral potentials with higher momentum-space cutoffs produce results closer to the ones based on (harder) phenomenological potentials and also to experimental data. This pattern is to be expected and provides an illustration of how a part of the intermediate-range contribution to the amplitude is reshuffled into the contact interaction upon explicitly integrating out the momentum components of the nucleons above the scale Λ_{NN}. The result for the chiral potential with a cutoff $R = 0.8$ fm is rather close to the result using AV18, cf. the left panels of Figs. 2 and 6. Finally, we remark that our results using the complete set of operators up-to-and-including NNLO are similar to the ones at LO. In other words, the inclusion of all LO, NLO and NNLO terms does not change the chiral NN potential cutoff pattern displayed in Fig. 6 right.

Finally, in Fig. 7 we plot the $|M_{^3P1}|$ amplitude, where the NN initial and final state wave functions are generated based on the N^{3}LO [52] and N^{4}LO [58] NN potentials, with the regulator $R = 0.9$ fm, which was found to yield the smallest theoretical uncertainties for NN observables. Interestingly, we observe a significant sensitivity of the calculated amplitude to the intermediate-range components of the NN potential.[5] We emphasize, that the results obtained using the N^{4}LO chiral NN wave functions lie closer to the experimental data and therefore yield more natural values for the NNLO contact term contribution. The difference between the two results is comparable in size to the cutoff variation discussed above.

VII. SUMMARY

Pion production in $pp \to d\pi^+$ reaction is studied at threshold within chiral EFT. Using a complete set of pion production operators derived in Refs. [14, 15] up-to-and-including next-to-next-to-leading order (NNLO) for s-wave pions and a set of modern phenomenological

[5] In addition to the isospin-breaking contact interaction in the ^{1}S$_0$ channel, the only new ingredient in the NN potential at N^{4}LO of Ref. [58] is given by the corresponding (parameter-free) two-pion exchange contributions.

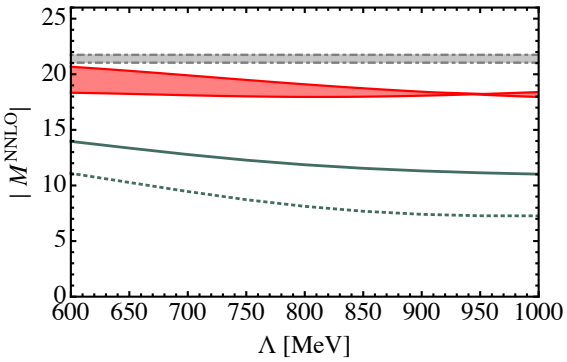

FIG. 7: The $pp \to d\pi^+$ amplitude $|M_{3P1}|$ from the complete set of LO, NLO and NNLO operators without any contact term in the $NN \to NN\pi$ transition operator as a function of the sharp momentum integral cutoff Λ for the NN potentials at N^{3}LO [52] (dotted line) and N^{4}LO [58] (solid line) corresponding to the choice of the regulator of $R = 0.9$ fm. The (red) band is the same as in Fig. 4, for notation of the horizontal grey band see Fig. 2.

and chiral NN potentials we calculate the threshold observable, namely the absolute value of the $pp \to d\pi^+$ reaction amplitude, and compare it to the experimental data. We emphasize that up to next-to-leading order our results are parameter free while at NNLO there is one unknown $NN \to NN\pi$ contact term. Apart from the description of data, the goal of this study was to demonstrate that the momentum counting scheme (MCS) used to classify the operators is adequate and that the theoretical uncertainty can be estimated reliably based on our expansion parameter. In particular, our results at NNLO serve to comply with this goal. Another goal of this work was to incorporate the $\Delta(1232)$ resonance in the analysis in order to investigate its role as an explicit degree of freedom for pion production reactions. Furthermore, we studied the sensitivity of the results to various NN wave functions.

As is known from the previous studies, the results in the $pp \to d\pi^+$ channel are governed by the longest range Weinberg-Tomozawa operator at leading order (LO) (see the top row in Fig.1) which alone yields the amplitude comparable to the experimental data. This result appears to be nearly independent of the NN model used. The contributions at next-to-leading order (NLO) undergo significant cancellations: while most of the loop contributions including pions, nucleons and Δ vanish exactly at this order, destructive interference of the diagrams which possess a (reducible) $N\Delta$ intermediate state (see diagrams dirΔa and ΔBox a in Fig.1), is not exact yielding a finite but small contribution comparable in size with the NNLO corrections. We observe that the available chiral potentials are generated with a cutoff, which tends to remove a part of the intermediate range physics relevant for the reaction $NN \to NN\pi$. On the other hand, we demonstrated that when the NN wave functions are calculated based on phenomenological potentials, which by construction take momenta significantly larger than the momentum scale inherent for pion production in $NN \to NN\pi$, the size of the contributions at LO, NLO and NNLO turns out to be in agreement with the expectations of the momentum counting scheme. Further, we find that the variation in the NNLO results due to the use of different πN low-energy constants (LECs) c_i is consistent with the uncertainty estimate expected at NNLO. In addition, some higher-order corrections from the nucleon recoil terms in the πNN propagators of the rescattering operators were evaluated explicitly to confirm that they are fully in line with the MCS estimate.

Apart from the state-of-the-art calculation of $pp \to d\pi^+$ reaction, the results of this work provide an important step towards a quantitative understanding of the much more challenging $pp \to pp\pi^0$ channel. The consistency of the power counting verified with the explicit calculations presented in this work (at least for phenomenological NN wave functions) is a necessary pre-requisite for studying the chirally suppressed neutral pion production.

Finally, the role of the Δ resonance was studied using three different strategies: (i) the most complete formulation with Δ-excitations being included in the Hilbert space which results in a coupled-channel framework (CCχEFT$-\Delta$) (ii) a perturbative treatment of Δ, where all effects associated with the Δ-nucleon mass difference are included in the pion production operator while the Hilbert space consists of only nucleonic states (χEFT$-\Delta$); (iii) Δ-less formulation of chiral EFT (χEFT$-\not{\Delta}$) where all effects due to the Δ isobar are integrated out and included in the LECs c_i.

We find that the difference between the approaches CCχEFT$-\Delta$ and χEFT$-\Delta$ does not exceed the magnitude of NNLO effects, if the cutoff is chosen in the range, which allows for a sufficient separation of the soft and hard scales ($\Lambda \geq 700$ MeV). Furthermore, the difference between the Δ-full and Δ-less approaches, which is expected to be of the size of the NLO corrections, is also comparable with the NNLO estimate. The smaller than expected difference can be attributed to destructive interference between the individually sizeable diagrams at NLO involving a (reducible) $N\Delta$ intermediate state.

VIII. ACKNOWLEDGMENTS

We thank Arnoldas Deltuva for providing us with the amplitudes generated from the CD Bonn NN model with explicit Δ's. This work was supported by the DFG (SFB/TR 16, "Subnuclear Structure of Matter"), the European Research Council (ERC-2010-StG 259218 NuclearEFT) and the National Science Foundation Grant No. PHY-1068305. This work was partially supported through GAUSTEQ (Germany and U.S. Nuclear Theory Exchange Program for QCD Studies of Hadrons and Nuclei) under contract number de-sc0006758. One of the authors (V.B.) thanks the DFG (grant GZ: BA 5443/1-1 AOBJ: 616443) for the partial support.

Appendix A: Pion production operator up to NNLO

In this appendix we list, for the sake of completeness, the operators for s-wave pion production from the diagrams shown in Fig. 1 up-to-and-including NNLO in the χEFT$-\Delta$ framework. Here we present the renormalized result for the threshold production operators. Details of the renormalization procedure can be found in Refs. [14, 15], where these operators were derived.

In the MCS, the rescattering operator at LO involves the Weinberg-Tomozawa πN vertex (including its recoil correction) which yields

$$iM^{\rm LO}_{\rm rescat} = \frac{g_A\,(2m_N)^2}{4f_\pi^3}\frac{m_\pi}{2\omega(k)}\left(\frac{1}{P_1}+\frac{1}{P_2}\right)(\vec{\sigma}_2\cdot\vec{k})\tau^a_\times + (1\leftrightarrow 2), \tag{A1}$$

where $f_\pi = 92.4$ MeV is the pion decay constant, $g_A = 1.32$ is the axial constant, and the pion propagator is written in terms of time-order-perturbation-theory (TOPT) (for details see Eqs.(A5) below). Here, $\tau^a_\times$ is the antisymmetric isospin operator, $\tau^a_\times = i(\boldsymbol{\tau}_1\times\boldsymbol{\tau}_2)^a$, with

the superscript a (a=1,2,3) referring to the isospin quantum number of the outgoing pion field, $\vec{\sigma}$ is a three-vector of Pauli matrices and $k_i = p_i - p_i'$, where p_i (p_i') stands for the momentum of the initial (final) nucleon i ($i = 1, 2$). The nucleon bispinors are normalized as $\bar{u}u = 2m_N$ which accounts for the appearance of a factor $(2m_N)^2$ in the amplitude (A1) and similar factors in the other amplitudes below. We note further that in the center of mass system the kinematics relevant for threshold pion production reads

$$\vec{p}_1 = -\vec{p}_2 =: \vec{p}, \quad \vec{p}_1' = -\vec{p}_2' =: \vec{p}', \quad \vec{k}_1 = -\vec{k}_2 =: \vec{k}\,. \tag{A2}$$

The interchange ($1 \leftrightarrow 2$) in Eq. (A1) (and the expressions below) indicates that the permutations of the initial and final nucleons need to be included (one needs also to take into account that $\vec{k} \to -\vec{k}$ under this interchange).

The tree-level rescattering operator at NNLO is decomposed into two parts: the first part, $M^{\rm NNLO}_{\rm rescat1}$, contains the corrections suppressed as $1/m_N$ due to the vertices from $\mathcal{L}^{(2)}_{\pi N}$ while the second term, $M^{\rm NNLO}_{\rm rescat2}$, accounts for the corrections $\propto 1/m_N^2$ from $\mathcal{L}^{(3)}_{\pi N}$.

The explicit TOPT expressions read

$$\begin{aligned}
iM^{\rm NNLO}_{\rm rescat1} &= \frac{g_A\,(2m_N)^2}{2f_\pi^3}\tau_2^a(\vec{\sigma}_2\cdot\vec{k})\left[\frac{4c_1m_\pi^2}{2\omega(k)}\left(\frac{1}{P_1}+\frac{1}{P_2}\right)-\left(2c_2+2c_3-\frac{g_A^2}{4m_N}\right)\frac{m_\pi}{2}\left(\frac{1}{P_1}-\frac{1}{P_2}\right)\right] \\
&- \frac{g_A\,(2m_N)^2}{2f_\pi^3}m_\pi\,\tau_\times^a\,\frac{\vec{\sigma}_2\cdot(\vec{p}+\vec{p}')}{4m_N}\frac{1}{2}\left(\frac{1}{P_1}-\frac{1}{P_2}\right)+(1\leftrightarrow 2), \qquad\qquad (A3)\\
iM^{\rm NNLO}_{\rm rescat2} &= -\frac{g_A(2m_N)^2}{2f_\pi^3}\frac{m_\pi}{2\omega(k)}\left(\frac{1}{P_1}+\frac{1}{P_2}\right)\left\{\tau_2^a\,(\vec{\sigma}_2\cdot\vec{k})\,\frac{\vec{p}^{\,2}-\vec{p}^{\,\prime 2}}{m_N^2}\left(m_Nc_2-\frac{g_A^2}{16}\right)\right. \\
&- \tau_\times^a\,(\vec{\sigma}_2\cdot\vec{k})\left[\frac{\vec{p}^{\,2}+\vec{p}^{\,\prime 2}}{16m_N^2}-\left(\frac{1+g_A^2+8m_Nc_4}{8m_N^2}\right)\left(i\vec{\sigma}_1\cdot(\vec{p}\times\vec{p}')-\frac{m_\pi^2}{2}\right)\right] \\
&- \left.\frac{\tau_\times^a}{8m_N^2}\left[(\vec{\sigma}_2\cdot\vec{p}')\vec{p}^{\,2}-(\vec{\sigma}_2\cdot\vec{p})\vec{p}^{\,\prime 2}\right]\right\} \\
&+ \frac{g_A(2m_N)^2}{4f_\pi^3}m_\pi\tau_\times^a\,(\vec{\sigma}_2\cdot\vec{k})\frac{1+g_A^2+8m_Nc_4}{8m_N^2}+(1\leftrightarrow 2). \qquad\qquad (A4)
\end{aligned}$$

To arrive at the expressions (A1), (A3) and (A4), we used that the pion propagator in TOPT reads

$$\frac{1}{k_2^2-m_\pi^2+i0} = \frac{1}{2\omega(k)}\left(\frac{1}{P_1}+\frac{1}{P_2}\right), \qquad \frac{v\cdot k_2}{k_2^2-m_\pi^2+i0} = \frac{1}{2}\left(\frac{1}{P_1}-\frac{1}{P_2}\right), \tag{A5}$$

$$P_1 = \sqrt{s}-2m_N-\frac{\vec{p}^{\,2}}{2m_N}-\frac{\vec{p}^{\,\prime 2}}{2m_N}-\omega(k), \tag{A6}$$

$$P_2 = \sqrt{s}-2m_N-m_\pi-\frac{\vec{p}^{\,2}}{2m_N}-\frac{\vec{p}^{\,\prime 2}}{2m_N}-\omega(k), \tag{A7}$$

where $\sqrt{s} = m_d + m_\pi$, $\omega(k) = \sqrt{m_\pi^2+\vec{k}^2}$ and $v\cdot k_2$ stands for the zeroth component of the four-vector k_2. Note that the leading effect from the propagators stems from the pion three-momentum squared, whereas the nucleon recoils are suppressed by two orders in the MCS. In order to retain all terms at NNLO, one therefore needs to keep the recoil terms in the leading Weinberg-Tomozawa operator (A1). Meanwhile, in the operators (A3) and

(A4), which start to contribute at NNLO, it suffices to preserve only the leading term in the propagators. However, we retain the recoil terms in the evaluations of these operators to maintain the correct analytic structure of the three-body propagators and to have an estimate of higher order terms. We find that the combined effect from all the recoil terms in Eqs.(A3) and (A4) is about 2% of the leading order amplitude, in full agreement with the estimate of N^{4}LO corrections.

Furthermore, we emphasize that the very last term in Eq. (A4) has the form which coincides exactly with the structure of the NNLO $NN \to NN\pi$ contact operator (see diagram in the last row in Fig. 1). Indeed, the contact term contribution for s-wave pion production in $pp \to d\pi^+$ reaction channel can be written as

$$iM_{\rm CT}^{\rm NNLO} = \frac{(2m_N)^2}{f_\pi^3} m_\pi \, C \, (\vec{\sigma}_2 \cdot \vec{k}) \tau_\times^a \, + (1 \leftrightarrow 2), \tag{A8}$$

where the renormalized part of the LEC C is of the order of Λ_χ^{-2} while its divergent part cancels the divergent terms from the NNLO loop contributions, as discussed in Refs. [14, 15] (see also a review article [2]). Since the details of the short-range mechanisms can not be revealed in an EFT study, it is convenient to absorb the last term in Eq. (A4) into the redefinition of the LEC C. The results presented in this paper are therefore obtained using this formulation. We note, however, that keeping the last term in Eq. (A4) explicitly is equally justified and does not affect the conclusions about the applicability of the MCS power counting drawn in this paper. For the results obtained in the formulation where the last term in Eq. (A4) is retained, the interested reader is referred to Ref. [61].

In addition to the rescattering operators, there are the so-called direct diagrams which respond for the direct pion emission from a single nucleon, see the first diagram in the first (fifth) row of Fig. 1, which contributes at LO (NNLO).

The contribution of the "direct" diagrams to the pion production operator is a one-nucleon operator and can be written as

$$\begin{aligned} iM_{\rm dir} \; = \; & \frac{g_A \, (2m_N)}{f_\pi} \tau_1^a \, m_\pi (2\pi)^3 \delta(\vec{p} - \vec{p}\,') \\ & \times \left[\frac{1}{4m_N} \vec{\sigma}_1 \cdot (\vec{p} + \vec{p}\,') - \frac{1}{16 m_N^3} \left(\vec{p}^{\,2} (\vec{\sigma}_1 \cdot \vec{p}) + \vec{p}^{\,\prime 2} (\vec{\sigma}_1 \cdot \vec{p}\,') \right) \right] + (1 \leftrightarrow 2) \, . \end{aligned} \tag{A9}$$

As explained in Ref. [15], this amplitude contributes to observables only when convoluted with the initial and final NN wave functions.

Further, the pion production operator contains diagrams with the intermediate $N\Delta$ state shown in the second row in Fig. 1. The diagrams "DirΔa" and the box diagram "ΔBox a" give rise to the contributions relevant for the $pp \to d\pi^+$ channel while all four diagrams contribute to $pp \to pp\pi^0$. These diagrams should be added to the operator derived in Ref. [15] if the Δ contributes as a part of the $NN \to NN\pi$ operator, i.e. in the χEFT$-\Delta$ framework. On the other hand, when the $N\Delta$ state is included in the coupled-channel formalism the contributions of these diagrams are generated automatically when the $N\Delta \to NN\pi$ ($NN \to N\Delta\pi$) operators shown in Fig. 5 are convolved with the initial state $NN \to N\Delta$ (final state $N\Delta \to NN$) amplitude. The diagrams in the second row in Fig. 1, therefore, should be omitted in the CCχEFT$-\Delta$ approach.

The expression for the "direct" diagram DirΔa in Fig. 1 reads

$$iM^{\rm NLO}_{\rm Dir\Delta a} = -\frac{g_A\, g^2_{\pi N\Delta}\,(2m_N)^2}{2f_\pi^3}\frac{m_\pi}{m_N}(\vec\sigma_2\cdot\vec k)\left(\frac{2}{3}(\vec p\,'\cdot\vec p-\vec p\,'^2)-\frac{i}{3}\vec\sigma_1\cdot(\vec p\,'\times\vec p)\right)\left(\frac{1}{3}\tau^a_\times+\frac{2}{3}\tau^a_2\right)$$
$$\times\frac{1}{\sqrt{s}-2m_N-\delta-\frac{\vec p\,'^2}{m_N}}\,\frac{1}{\vec k^2+m_\pi^2}+(1\leftrightarrow 2), \tag{A10}$$

where $\delta=m_\Delta-m_N$, the first propagator stands for the TOPT propagator corresponding to the $N\Delta$ intermediate state while the second one corresponds to the static OPE propagator in the $NN\to N\Delta$ transition. Although the term $\sim m_\pi^2$ in the OPE propagator gives rise to higher-order effects at next-to-next-to-next-to-leading order (NNNLO), we keep it to allow for a close comparison with our results based on a coupled-channel approach (see Sec. V B for a detailed discussion of the results). In particular, in order to obtain the results in the coupled-channel framework (CCχEFT$-\Delta$) we utilized the $NN\to N\Delta$ transition amplitude generated in Ref. [36] using iterations of the static OPE potential. We checked that neglecting the term $\sim m_\pi^2$ in the OPE propagator results in an about 3% correction to the reaction amplitude which is fully in line with NNNLO estimate. Further, for the purpose of study $NN\to NN\pi$ reaction near threshold to the order we are working, the width of the Δ-resonance in the propagators can be safely neglected: while the Δ width vanishes exactly at pion production threshold, it constitutes a higher order effect for the energies near threshold.

The expression for the box diagrams "ΔBox a" and "ΔBox b" (the second row in Fig. 1) is

$$iM^{\rm NLO}_{\Delta\rm box} = \frac{g_A g^2_{\pi N\Delta}\,(2m_N)^2}{36f_\pi^5}\,m_\pi\left[3\tau^a_+\,i\vec k\cdot(\vec\sigma_1\times\vec\sigma_2)\left(I_{\rm sum}-\frac{1}{4}\frac{\vec k^2}{\delta}(J_{\pi\pi\Delta}+J_{\pi\pi N})\right)\right.$$
$$\left.-(\vec\sigma_1+\vec\sigma_2)\cdot\vec k\,\tau^a_\times\left(I_{\rm sum}-\frac{1}{2}\frac{\vec k^2}{\delta}(J_{\pi\pi\Delta}+J_{\pi\pi N})\right)\right]+(1\leftrightarrow 2), \tag{A11}$$

where $g_{\pi N\Delta}=1.34$ is the leading $\pi N\Delta$ coupling constant, τ^a_+ is the symmetric isospin operator, $\tau^a_+=(\boldsymbol{\tau}_1+\boldsymbol{\tau}_2)^a$, and the integral combination $I_{\rm sum}$ is

$$I_{\rm sum}=I_{\pi\pi}+\frac{1}{2}\frac{J_{\pi\Delta}}{\delta}+\delta J_{\pi\pi\Delta}+\frac{2}{(4\pi)^2}. \tag{A12}$$

The individual integrals are defined below, see Eqs. (A15–A18). Note that the integrals $I_{\rm sum}, J_{\pi\pi\Delta}$ and $J_{\pi\pi N}$ are finite ($I_{\rm sum}$ and $\frac{1}{\delta}(J_{\pi\pi\Delta}+J_{\pi\pi N})$ vanish in the limit $\delta\to\infty$) while the divergent part of the loop is absorbed in the $NN\to NN\pi$ contact term contribution at NNLO, see Eq. (A8).

The contribution of pion-nucleon loops to the production operator for s-wave pions was derived in Ref. [14]. After renormalization the finite part of these loops reads

$$iM^{\rm NNLO}_{\pi N-\rm loops} = -\frac{g_A\,(2m_N)^2\,m_\pi}{4f_\pi^5}\tau^a_\times(\vec\sigma_1+\vec\sigma_2)\cdot\vec k\left[\frac{1}{6}I^R_{\pi\pi}(k_1^2)\left(1-\frac{19}{4}g_A^2\right)-\frac{1}{18(4\pi)^2}\left(1-10g_A^2\right)\right]$$
$$-\,i\,\frac{g_A^3\,(2m_N)^2\,m_\pi}{4f_\pi^5}\tau^a_+\,\vec k\cdot(\vec\sigma_1\times\vec\sigma_2)\,I^R_{\pi\pi}(k_1^2)+(1\leftrightarrow 2), \tag{A13}$$

where the integral $I^R_{\pi\pi}(k_1^2)$ is defined below, see Eq. (A19)[6].

Finally, the renormalized, finite Δ loop diagrams contribution to s-wave pion production at NNLO reads:

$$\begin{aligned} iM^{\rm NNLO}_{\Delta\text{-loops}} &= -\frac{g_A g^2_{\pi N\Delta}\,(2m_N)^2}{4f_\pi^5}\, m_\pi\, \tau_\times\, (\vec\sigma_1+\vec\sigma_2)\cdot\vec k \\ &\times \left[\frac{5}{9}I_{\rm sum} - \frac{1}{18}\vec k^2 J_{\pi\pi N\Delta} - \frac{8}{9}\frac{\delta^2}{\vec k^2} I_{\rm sum} - \frac{2}{27}\left(I_{\pi\pi} + \frac{1}{2}\frac{J_{\pi\Delta}}{\delta} + \frac{1}{3}\frac{2}{(4\pi)^2}\right)\right] \\ &+ i\frac{g_A g^2_{\pi N\Delta}\,(2m_N)^2}{8f_\pi^5} m_\pi\, \tau^a_+\, \vec k\cdot(\vec\sigma_1\times\vec\sigma_2)\left[\frac{2}{9}I_{\rm sum} - \frac{1}{18}\vec k^2 J_{\pi\pi N\Delta}\right] + (1\leftrightarrow 2). \quad \text{(A14)} \end{aligned}$$

The dimensionless loop integrals entering Eqs. (A11), (A13) and (A14) are defined as follows

$$\frac{1}{\delta}J_{\pi\Delta}(\delta) = \frac{\mu^\epsilon}{i\delta}\int\frac{d^{4-\epsilon}l}{(2\pi)^{4-\epsilon}}\frac{1}{(l^2-m_\pi^2+i0)(-v\cdot l-\delta+i0)}\,, \quad \text{(A15)}$$

$$I_{\pi\pi}(k_1^2) = \frac{\mu^\epsilon}{i}\int\frac{d^{4-\epsilon}l}{(2\pi)^{4-\epsilon}}\frac{1}{(l^2-m_\pi^2+i0)((l+k_1)^2-m_\pi^2+i0)}\,, \quad \text{(A16)}$$

$$\delta J_{\pi\pi\Delta}(k_1^2,\delta) = \delta\frac{\mu^\epsilon}{i}\int\frac{d^{4-\epsilon}l}{(2\pi)^{4-\epsilon}}\frac{1}{(l^2-m_\pi^2+i0)((l+k_1)^2-m_\pi^2+i0)(-v\cdot l-\delta+i0)}, \quad \text{(A17)}$$

$$\vec k^2 J_{\pi\pi N\Delta}(k_1^2,\delta) = \frac{\vec k^2}{\delta}(J_{\pi\pi\Delta}-J_{\pi\pi N}), \quad \text{(A18)}$$

where $J_{\pi\pi N}(k_1^2) = J_{\pi\pi\Delta}(k_1^2,\delta=0)$. The integrals (A17) and (A18) as well as the linear combination $I_{\rm sum}$ from Eq. (A12) are finite and were evaluated numerically, while the integrals $J_{\pi\Delta}$ and $I_{\pi\pi}$ contain finite and divergent parts. The renormalized finite parts of $J_{\pi\Delta}$ and $I_{\pi\pi}$ are given by [15]:

$$I^R_{\pi\pi} = -\frac{1}{(4\pi)^2}\log\left(\frac{m_\pi^2}{\mu^2}\right) + \frac{1}{(4\pi)^2}\left(1 - 2\frac{\sqrt{4-x-i0}}{\sqrt{x}}\arctan\left(\frac{\sqrt{x}}{\sqrt{4-x-i0}}\right)\right), \quad \text{(A19)}$$

$$\frac{1}{\delta}J^R_{\pi\Delta} = \frac{2}{(4\pi)^2}\log\left(\frac{m_\pi^2}{\mu^2}\right) + \frac{4}{(4\pi)^2}\left\{-\frac{1}{2} + \frac{\sqrt{1-y-i0}}{\sqrt{y}}\left[-\frac{\pi}{2} + \arctan\left(\frac{\sqrt{y}}{\sqrt{1-y-i0}}\right)\right]\right\}, \quad \text{(A20)}$$

where μ is the dimension-regularization scale which is chosen to be $\mu \simeq 4\pi f_\pi (\simeq \Lambda_\chi \simeq m_N)$ in our calculation.[7] Furthermore, the variables x, y are defined as $x = k_1^2/m_\pi^2$, $y = \delta^2/m_\pi^2$. The permutations $(1\leftrightarrow 2)$ in the expressions above would result in a symmetry factor of four, once the operators are projected onto the partial wave ${}^3P_1 \to ({}^3S_1 - {}^3D_1)s$ relevant for the $pp\to d\pi^+$ reaction. Further, in order to obtain the observables, the operators above need to be convoluted with the initial NN and final deuteron wave functions. The technical details of this procedure were discussed in Ref. [15] (see appendix A).

[6] In Ref. [14], the integral $I_{\pi\pi}(k_1^2)$ was called $J(k_1^2)$.

[7] The μ-dependence in the above expressions is absorbed into the five-point contact term [15] whose contributions to the pion production amplitude is not included in the shown results.

Appendix B: Additional $N\Delta \to NN\pi$ operators in the coupled-channel approach

The expressions for the tree-level diagrams involving an initial or final state Δ resonance, as shown in Fig. 5, read

$$\begin{aligned}
iM_{\rm dir\Delta a} &= \frac{g_{\pi N\Delta}\,(2m_N)}{m_N f_\pi}\,T_1^a\,m_\pi\,(\vec{S}_1\cdot\vec{p})(2\pi)^3\delta(\vec{p}-\vec{p}\,'),\\
iM_{\rm dir\Delta b} &= \frac{g_{\pi N\Delta}\,(2m_N)}{m_N f_\pi}\,T_1^{\dagger a}\,m_\pi\,(\vec{S}_1^{\,\dagger}\cdot\vec{p}\,')(2\pi)^3\delta(\vec{p}-\vec{p}\,'),\\
iM_{\rm rescat\Delta a} &= \frac{g_{\pi N\Delta}\,(2m_N)^2}{2f_\pi^3}\,i\epsilon^{bac}\tau_1^c T_2^b\,\frac{m_\pi}{2\omega(k)}\left(\frac{1}{P_1}+\frac{1}{P_{2\Delta}}\right)(\vec{S}_2\cdot\vec{k}),\\
iM_{\rm rescat\Delta b} &= \frac{g_{\pi N\Delta}\,(2m_N)^2}{2f_\pi^3}\,i\epsilon^{bac}\tau_1^c T_2^{\dagger b}\,\frac{m_\pi}{2\omega(k)}\left(\frac{1}{P_{1\Delta}}+\frac{1}{P_2}\right)(\vec{S}_2\cdot\vec{k}),
\end{aligned}\tag{B1}$$

where $\vec{S}$ and $\mathbf{T}$ are the spin and isospin transition matrices, normalized such that

$$S_i S_j^\dagger = \frac{1}{3}\left(2\delta_{ij} - i\epsilon_{ijk}\,\sigma_k\right), \quad T_i T_j^\dagger = \frac{1}{3}\left(2\delta_{ij} - i\epsilon_{ijk}\,\tau_k\right), \quad i,j=1,2,3. \tag{B2}$$

Furthermore, the TOPT propagators read

$$\begin{aligned}
P_{1\Delta} &= \sqrt{s} - 2m_N - \delta - \frac{\vec{p}^{\,2}}{2m_N} - \frac{\vec{p}\,'^2}{2m_N} - \omega(k),\\
P_{2\Delta} &= \sqrt{s} - 2m_N - m_\pi - \delta - \frac{\vec{p}^{\,2}}{2m_N} - \frac{\vec{p}\,'^2}{2m_N} - \omega(k).
\end{aligned}\tag{B3}$$

Clearly, the operators (B1) contribute to the reaction amplitude of $NN \to NN\pi$ only when they are inserted as a building block into those of final- and initial-state interaction diagrams which have an $N\Delta$ intermediate state like in our coupled-channel treatment (CCχEFT$-\Delta$). As already explained, to avoid double counting, in this case the contributions of the diagrams in the second row in Fig. 1 should not be included.

---

[1] C. Hanhart, Phys. Rept. **397** (2004) 155.
[2] V. Baru, C. Hanhart and F. Myhrer, Int. J. Mod. Phys. E **23** (2014) 4, 1430004.
[3] C. Hanhart, U. van Kolck and G. A. Miller, Phys. Rev. Lett. **85**, (2000) 2905.
[4] V. Baru, E. Epelbaum, J. Haidenbauer, C. Hanhart, A. E. Kudryavtsev, V. Lensky and U.-G. Meißner, Phys. Rev. C **80**, (2009) 044003.
[5] U. van Kolck, Phys. Rev. C **49**, (1994) 2932.
[6] E. Epelbaum, A. Nogga, W. Gloeckle, H. Kamada, U.-G. Meißner and H. Witala, Phys. Rev. C **66**, (2002) 064001.
[7] D. S. Koltun and A. Reitan, Phys. Rev. **141** (1966) 1413.
[8] H. O. Meyer *et al.*, Nucl. Phys. A **539** (1992) 633.
[9] T. D. Cohen, J. L. Friar, G. A. Miller and U. van Kolck, Phys. Rev. C **53** (1996) 2661.
[10] B. Y. Park, F. Myhrer, J. R. Morones, T. Meissner and K. Kubodera, Phys. Rev. C **53** (1996) 1519.

[11] T. Sato, T. S. H. Lee, F. Myhrer and K. Kubodera, Phys. Rev. C **56** (1997) 1246.
[12] C. Hanhart and N. Kaiser, Phys. Rev. C **66** (2002) 054005.
[13] V. Lensky, V. Baru, J. Haidenbauer, C. Hanhart, A. E. Kudryavtsev and U.-G. Meißner, Eur. Phys. J. A **27** (2006) 37.
[14] A. A. Filin, V. Baru, E. Epelbaum, H. Krebs, C. Hanhart, A. E. Kudryavtsev and F. Myhrer, Phys. Rev. C **85** (2012) 054001.
[15] A. A. Filin, V. Baru, E. Epelbaum, H. Krebs, C. Hanhart and F. Myhrer, Phys. Rev. C **88** (2013) 064003.
[16] G. A. Miller, A. K. Opper and E. J. Stephenson, Ann. Rev. Nucl. Part. Sci. **56** (2006) 253.
[17] A. K. Opper *et al.*, Phys. Rev. Lett. **91** (2003) 212302.
[18] U. van Kolck, J. A. Niskanen and G. A. Miller, Phys. Lett. B **493** (2000) 65.
[19] D. R. Bolton and G. A. Miller, Phys. Rev. C **81** (2010) 014001.
[20] A. Filin, V. Baru, E. Epelbaum, J. Haidenbauer, C. Hanhart, A. E. Kudryavtsev and U.-G. Meißner, Phys. Lett. B **681** (2009) 423.
[21] T. Strauch *et al.*, Phys. Rev. Lett. **104** (2010) 142503.
[22] T. Strauch *et al.*, Eur. Phys. J. A **47** (2011) 88.
[23] S. Weinberg, Phys. Lett. B **295** (1992) 114.
[24] C. Hanhart, J. Haidenbauer, M. Hoffmann, U.-G. Meißner and J. Speth, Phys. Lett. B **424** (1998) 8.
[25] V. Dmitrasinovic, K. Kubodera, F. Myhrer and T. Sato, Phys. Lett. B **465** (1999) 43.
[26] S.-i. Ando, T.-S. Park and D. P. Min, Phys. Lett. B **509** (2001) 253.
[27] V. Bernard, N. Kaiser and U.-G. Meißner, Eur. Phys. J. A **4** (1999) 259.
[28] Y. Kim, T. Sato, F. Myhrer and K. Kubodera, Phys. Lett. B **657**, (2007) 187.
[29] Y. Kim, T. Sato, F. Myhrer and K. Kubodera, Phys. Rev. C **80**, (2009) 015206.
[30] C. da Rocha, G. Miller and U. van Kolck, Phys. Rev. C **61** (2000) 034613.
[31] V. Baru, J. Haidenbauer, C. Hanhart, A. E. Kudryavtsev, V. Lensky and U.-G. Meißner, in *Proceedings of 11-th International Conference on Meson-Nucleon Physics and the Structure of the Nucleon (MENU 2007), Jülich, Germany*, eConfC **070910** 128 (2007); [arXiv:0711.2748 [nucl-th]].
[32] J. A. Niskanen, Nucl. Phys. A **298**, (1978) 417.
[33] C. Hanhart, J. Haidenbauer, O. Krehl and J. Speth, Phys. Lett. B **444** (1998) 25.
[34] T. R. Hemmert, B. R. Holstein and J. Kambor, J. Phys. G **24**, (1998) 1831.
[35] V. Pascalutsa and D. R. Phillips, Phys. Rev. C **67**, (2003) 055202.
[36] A. Deltuva, R. Machleidt and P. U. Sauer, Phys. Rev. C **68**, (2003) 024005.
[37] J. Haidenbauer, K. Holinde and M. B. Johnson, Phys. Rev. C **48**, (1993) 2190.
[38] V. Baru, J. Haidenbauer, C. Hanhart, A. E. Kudryavtsev, V. Lensky and U.-G. Meißner, Phys. Lett. B **659**, (2008) 184.
[39] V. Baru, C. Hanhart, M. Hoferichter, B. Kubis, A. Nogga and D. R. Phillips, Nucl. Phys. A **872**, (2011) 69.
[40] V. Baru, C. Hanhart, M. Hoferichter, B. Kubis, A. Nogga and D. R. Phillips, Phys. Lett. B **694**, (2011) 473.
[41] R. Machleidt, Phys. Rev. C **63** (2001) 024001.
[42] V. G. J. Stoks, R. A. M. Klomp, C. P. F. Terheggen and J. J. de Swart, Phys. Rev. C **49** (1994) 2950.
[43] R. B. Wiringa, V. G. J. Stoks and R. Schiavilla, Phys. Rev. C **51** (1995) 38.
[44] H. Krebs, E. Epelbaum and U.-G. Meißner, Eur. Phys. J. A **32**, (2007) 127.

[45] N. Fettes, U.-G. Meißner and S. Steininger, Nucl. Phys. A **640**, (1998) 199.
[46] H. Krebs, A. Gasparyan and E. Epelbaum, Phys. Rev. C **85**, (2012) 054006.
[47] N. Fettes and U.-G. Meißner, Nucl. Phys. A **676**, (2000) 311.
[48] J. M. Alarcon, J. Martin Camalich and J. A. Oller, Annals Phys. **336**, (2013) 413.
[49] Y. H. Chen, D. L. Yao and H. Q. Zheng, Phys. Rev. D **87**, (2013) 054019.
[50] K. A. Wendt, B. D. Carlsson and A. Ekström, arXiv:1410.0646 [nucl-th].
[51] D. Siemens, V. Bernard, E. Epelbaum, A. Gasparyan, H. Krebs and U.-G. Meißner, arXiv:1602.02640 [nucl-th].
[52] E. Epelbaum, H. Krebs and U.-G. Meißner, Eur. Phys. J. A **51** (2015) 5, 53.
[53] M. Hoferichter, J. Ruiz de Elvira, B. Kubis and U.-G. Meißner, Phys. Rev. Lett. **115**, (2015) 092301.
[54] M. Hoferichter, J. Ruiz de Elvira, B. Kubis and U.-G. Meißner, Phys. Rev. Lett. **115**, (2015) 192301.
[55] P. Büttiker and U.-G. Meißner, Nucl. Phys. A **668**, (2000) 97.
[56] V. Bernard, N. Kaiser and U.-G. Meißner, Nucl. Phys. A **615**, (1997) 483.
[57] E. Epelbaum, H. Krebs and U.-G. Meißner, Nucl. Phys. A **806**, (2008) 65.
[58] E. Epelbaum, H. Krebs and U.-G. Meißner, Phys. Rev. Lett. **115** (2015) 12, 122301.
[59] D. R. Entem and R. Machleidt, Phys. Rev. C **68**, (2003) 041001.
[60] E. Epelbaum, W. Glöckle and U.-G. Meißner, Nucl. Phys. A **747**, (2005) 362.
[61] A. A. Filin, V. Baru, E. Epelbaum, H. Krebs, C. Hanhart, and F. Myhrer, in *Proceedings of 8-th International Workshop on Chiral Dynamics (CD 2015), Pisa, Italy*, to be published.